

Non-spherical proton shape and hydrogen hyperfine splitting *

A. J. Buchmann
Institute for Theoretical Physics
University of Tübingen
D-72076 Tübingen, Germany[†]

We show that the non-spherical charge distribution of the proton manifests itself in hydrogen hyperfine splitting as an increase (in absolute value) of the proton Zemach radius and polarization contributions.

PACS numbers: 13.40.-f, 21.10.-k, 31.30.Gs

I. INTRODUCTION

Hydrogen hyperfine splitting (hfs), which is predominantly due to the interaction of electron and proton magnetic moments, is an interesting observable. It provides not only precision tests for quantum electrodynamics, but also valuable information on proton structure and strong interactions. According to Fermi's theory [1], the energy difference between the two hydrogen hyperfine states is

$$E_F = \frac{8}{3} \frac{\alpha^3}{\pi} \frac{m_e^3 m_p^3}{(m_e + m_p)^3} \mu_e \mu_p, \quad (1)$$

where α is the fine structure constant, m_e is the mass of the electron and μ_e its magnetic moment; m_p and μ_p are the proton mass and magnetic moment. Numerically, this gives $E_F = 1,418,840.11$ kHz using recent values for these fundamental constants [2].

The interplay between experiment and theory has been particularly fruitful in the case of hydrogen hfs. For example, when the original measurement [3] exceeded the prediction of Eq.(1) by 0.26 %, which was far more than the experimental accuracy at that time, this stimulated the first quantum electrodynamics (QED) calculation of the electron anomalous magnetic moment [4]. The latter was then identified as the major reason for the \sim MHz discrepancy between experiment and Fermi's formula. Further studies revealed that hydrogen hyperfine splitting is not only affected by global proton properties such as its mass, charge, and magnetic moment, but is also sensitive to the details of the spatial charge and current distributions in the proton and its excited states [5, 6]. These nucleon structure effects contribute to hfs at the level of several tens of kHz.

In the meantime, the transition frequency between the two hyperfine states has been measured [7] with an experimental uncertainty of about 1 mHz

$$E_{exp}^{HFS} = 1,420,405,751.7667 \pm 0.0009 \text{ [Hz]}, \quad (2)$$

corresponding to a relative accuracy of 10^{-12} . Thus, hydrogen ground state hfs is one of most precisely measured physical quantities. On the other hand, the accuracy of present calculations of nucleon structure effects in hydrogen hfs is at best of order 10^{-6} and hence many orders of magnitude lower than the precision with which the fundamental constants and QED corrections are known. Therefore, hydrogen hfs can be used as a high precision probe for investigating fine details of proton structure.

Another way of studying the structure of the nucleon is electron-nucleon scattering. Employing polarized electron beams and hydrogen targets, it has recently become possible to experimentally determine the $p \rightarrow \Delta^+(1232)$ charge quadrupole transition form factor [8]. It has been proposed that the quadrupole excitation of the nucleon $N(939)$ to the $\Delta(1232)$ resonance is closely related to a quadrupole deformation of the nucleon's ground state charge distribution as reflected by a positive intrinsic quadrupole moment [9] and an intrinsic charge quadrupole form factor [10]. This interpretation is based on relations between nucleon ground state and $N \rightarrow \Delta$ transition form factors that follow from broken strong interaction symmetries.

The purpose of this paper is to explore in which way and to what extent the proton's non-spherical charge density affects hydrogen hfs. As a spin 1/2 particle the proton does not have a spectroscopic quadrupole moment and its non-spherical charge distribution does not result in a quadrupole interaction term in the hfs energy shift formula [10]. Nevertheless, deviations from a spherically symmetric proton charge distribution are detectable in hydrogen hfs via the quadrupole excitation of the nucleon to the $\Delta^+(1232)$ resonance by the atomic electron (polarization shift) and via their effect on the electromagnetic size of the proton (Zemach radius).

The paper is organized as follows. In sect. II we discuss the electromagnetic $N \rightarrow \Delta$ transition and what we have learned from it about the geometric shape of the nucleon in some detail. In sect. III the implications of the nucleon's non-sphericity for the hydrogen atom hyperfine splitting are investigated. The paper closes with a summary of our results and an outlook.

*published in Can. J. Phys. **87**, 773 (2009).

[†]Electronic address: alfons.buchmann@uni-tuebingen.de

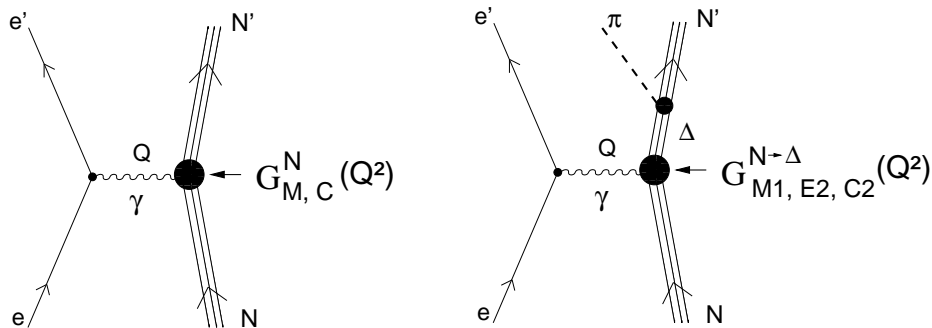


FIG. 1: Left: Probing of nucleon structure via elastic electron-nucleon scattering $e N \rightarrow e' N'$ involving the exchange of a single virtual photon γ of four-momentum $Q = (\nu, -\mathbf{q})$ with ν and \mathbf{q} being its energy and three-momentum transfer. Nucleon structure information is contained in the magnetic dipole form factor $G_M^N(Q^2)$ and charge monopole form factor $G_C^N(Q^2)$. Right: Inelastic electron-nucleon scattering $e N \rightarrow e' \Delta \rightarrow e' N' \pi$ (electro-pionproduction). The electromagnetic excitation of the $\Delta(1232)$ resonance is described by three transition form factors $G_{M1}^{N \rightarrow \Delta}(Q^2)$, $G_{E2}^{N \rightarrow \Delta}(Q^2)$, and $G_{C2}^{N \rightarrow \Delta}(Q^2)$.

II. ELECTROMAGNETIC $N \rightarrow \Delta$ TRANSITION AND NUCLEON SHAPE

A. Elastic and inelastic electron scattering

Nucleon structure information is encoded in two elastic electromagnetic form factors, namely the charge monopole $G_C^N(Q^2)$ and magnetic dipole $G_M^N(Q^2)$ form factors as indicated by the black dot in Fig. 1 (left). These form factors have been measured in elastic electron-proton and electron-deuteron (neutron) scattering experiments performed at various laboratories. In particular, it has been shown that the proton has a finite charge radius of about 0.9 fm [11]. In addition, the Fourier transforms of the elastic form factors have provided information on the radial variation of the charge $\rho(r)$ and current $\mathbf{j}(r)$ densities of the proton [12].

Inelastic electron-proton scattering with the production of a single pion (electro-pionproduction) has revealed that the proton has a rich spectrum of excited states [13]. Its lowest lying excited state with spin 3/2 and isospin 3/2, the $\Delta(1232)$ resonance, plays a special role because it has the largest production cross section and its properties are most closely related to those of the nucleon ground state $N(939)$. Parity invariance of the electromagnetic interaction and angular momentum conservation restrict the $N \rightarrow \Delta$ excitation to magnetic dipole (M1), electric quadrupole (E2), and charge or Coulomb quadrupole (C2) transitions with corresponding transition form factors as depicted by the large black dot in Fig. 1 (right). The nonzeroness of the C2 form factor indicates that the nucleon charge distribution is not spherically symmetric [8] but has an angular dependence $\rho(\mathbf{r}) = \rho(r, \Theta, \Phi)$. In the following we review the connection between the quadrupole excitation of the $\Delta(1232)$ resonance and nucleon ground state deformation using strong interaction symmetries as a guide.

B. Spin-flavor symmetry and electromagnetic form factor relations

Aside from SU(2) isospin and SU(3) flavor symmetries, strong interactions are also approximately invariant under the higher SU(6) spin-flavor symmetry. The latter unites the spin 1/2 flavor octet baryons (2×8 states), among them the familiar proton and neutron, and the spin 3/2 flavor decuplet baryons (4×10 states), including the four $\Delta(1232)$ states into a common **56**-dimensional mass degenerate supermultiplet [14]. We now understand that the underlying field theory of strong interactions, quantum chromodynamics (QCD), possesses a spin-flavor symmetry which is exact in the large N_c limit, where N_c denotes the number of colors. Moreover, for finite N_c , spin-flavor symmetry breaking operators can be classified according to the powers of $1/N_c$ associated with them. This leads to a perturbative expansion scheme for QCD processes that works at all energy scales [15].

For $N_c = 3$ we may just as well employ a parametrization method [16], which incorporates SU(6) symmetry and its breaking similar to the $1/N_c$ expansion. The basic idea is to write for the observable under investigation the most general spin-flavor operator. Generally, this is a sum of one-, two-, and three-quark operators in spin-flavor space multiplied by *a priori* unknown constants which parameterize the orbital and color space matrix elements, and which are determined from experiment. A multipole expansion of the nucleon charge density operator ρ in spin-flavor space up to quadrupole terms leads to the following invariants

$$\rho = \rho_{[1]} + \rho_{[2]} + \rho_{[3]} = A \sum_i^3 e_i \mathbf{1} - \left(B \sum_{i \neq j}^3 e_i + C \sum_{i \neq j \neq k}^3 e_k \right) \left[2 \underbrace{\sigma_i \cdot \sigma_j}_{\text{spin scalar}} - \underbrace{(3\sigma_{iz} \sigma_{jz} - \sigma_i \cdot \sigma_j)}_{\text{spin tensor}} \right], \quad (3)$$

where σ_{iz} is the z -component of the Pauli spin matrix of

quark i , and $e_i = \frac{1}{6}(1 + 3\tau_{iz})$ is the quark charge where τ_{iz} is the third component of the Pauli isospin matrix. The constants A , B , and C contained in the one-, two- and three-quark charge density operators parametrize the orbital and color matrix elements so that ρ is only an operator in spin-flavor space. The factors 2 and -1 in front of the spin scalar and spin tensor terms are dictated by group theory and reflect the fact that both terms arise from a common SU(6) spin-flavor tensor [10]. In terms of fundamental processes (see Fig. 2), the one-quark operator in Eq.(3) represents valence quarks whereas the two-, and three-quark operators provide an effective description of the quark-antiquark degrees of freedom in the N and Δ . For the two-body current in Fig. 2(b) this is explained in more detail in Ref. [17].

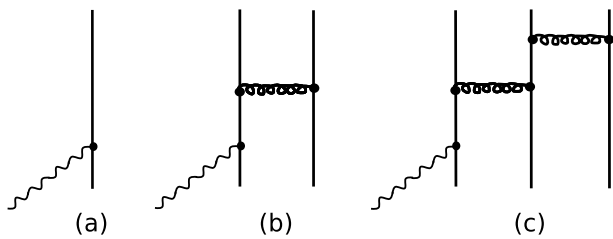


FIG. 2: Fundamental photon-quark processes contributing to the form factors in Fig. 1: (a) one-quark current ($\rho_{[1], \mathbf{j}_{[1]}}$), (b) two-quark gluon exchange current ($\rho_{[2], \mathbf{j}_{[2]}}$), (c) three-quark gluon exchange current ($\rho_{[3], \mathbf{j}_{[3]}}$).

Evaluating the charge operator in Eq.(3) between spin-flavor wave functions [18] of the **56** dimensional SU(6) ground state multiplet, in particular, for the neutron and between the initial proton and final Δ^+ states, leads to

$$\begin{aligned} r_n^2 &= \langle 56_n | \rho_{[2]} + \rho_{[3]} | 56_n \rangle = 4(B - 2C), \\ Q_{p \rightarrow \Delta^+} &= \langle 56_{\Delta^+} | \rho_{[2]} + \rho_{[3]} | 56_p \rangle = 2\sqrt{2}(B - 2C). \end{aligned} \quad (4)$$

Note that in this approach, valence quarks make no contribution and both observables are governed by quark-antiquark degrees of freedom in the nucleon. Hence, the following relation between the transition quadrupole moment $Q_{p \rightarrow \Delta^+}$ and the neutron charge radius r_n^2 is obtained

$$Q_{p \rightarrow \Delta^+} = \frac{1}{\sqrt{2}} r_n^2. \quad (5)$$

This relation was originally derived in the constituent quark model with two-quark exchange currents [19] and shown to hold after including three-quark operators [20]. It was found that Eq.(5) is the zero momentum transfer limit of a more general relation [21] between the $N \rightarrow \Delta$ charge quadrupole transition form factor $G_{C2}^{N \rightarrow \Delta}(Q^2)$ and

the elastic neutron charge form factor $G_C^n(Q^2)$

$$\begin{aligned} G_{C2}^{N \rightarrow \Delta}(Q^2) &= -\frac{3\sqrt{2}}{Q^2} G_C^n(Q^2), \\ Q_{N \rightarrow \Delta} &:= G_{C2}^{N \rightarrow \Delta}(0) = \frac{1}{\sqrt{2}} r_n^2, \\ r_{C2}^2 &= \frac{7}{10} \frac{r_n^4}{r_n^2}, \end{aligned} \quad (6)$$

which is valid for both the $p \rightarrow \Delta^+$ and $n \rightarrow \Delta^0$ transitions, and that the quadrupole transition radius is determined by the fourth and second radial moments of the neutron charge distribution.

In addition, SU(6) spin-flavor symmetry leads to the following relations [14] between the neutron ground state and the $N \rightarrow \Delta$ magnetic form factors $G_{M1}^{N \rightarrow \Delta}(Q^2) = -\sqrt{2} G_M^n(Q^2)$, and at $Q^2 = 0$ between the neutron and transition magnetic moments $\mu_{N \rightarrow \Delta} = -\sqrt{2} \mu_n$. With the help of Eq.(6) and the magnetic form factor relations, the C2/M1 ratio in electromagnetic $\Delta(1232)$ excitation can be expressed in terms of the neutron elastic form factors as follows [21]

$$\begin{aligned} \frac{C2}{M1}(Q^2) &:= \frac{|\mathbf{q}| m_N}{6} \frac{G_{C2}^{N \rightarrow \Delta}(Q^2)}{G_{M1}^{N \rightarrow \Delta}(Q^2)} = \frac{|\mathbf{q}| m_N}{2 Q^2} \frac{G_C^n(Q^2)}{G_M^n(Q^2)}, \\ \frac{C2}{M1}(0) &= \frac{(m_\Delta - m_N) m_N}{12} \frac{r_n^2}{\mu_n}, \end{aligned} \quad (7)$$

where $|\mathbf{q}|$ is the modulus of the photon's three-momentum and where m_N , m_Δ are the nucleon and Δ masses. The theoretical uncertainty of this relation is mainly due to third order SU(6) symmetry breaking operators of order $1/N_c^2$ (three-quark currents) violating the magnetic form factor relation. It is estimated that such correction terms could lead to 10% decrease of $|C2/M1|$.

C. Comparison with experiment

In Fig. 3, the experimental $C2/M1$ ratio as measured in electro-pionproduction is shown. The full curve represents the Maid 2007 analysis [22] of the world $C2/M1$ data, while the dashed-dotted line is based on Eq.(7) which relates the inelastic $N \rightarrow \Delta$ and the elastic neutron form factors. For definiteness we use a Galster parametrization [23]

$$\begin{aligned} G_C^n(Q^2) &= -a \frac{\tau}{1 + d\tau} G_M^n(Q^2), \quad \tau = \frac{Q^2}{4m_N^2}, \\ G_M^n(Q^2) &= \mu_n \left(1 + \frac{Q^2}{\Lambda_M^2} \right)^{-2} \end{aligned} \quad (8)$$

for the experimental neutron charge form factor, where $G_M^n(Q^2)$ is a dipole representation of the neutron magnetic form factor with Λ_M being the dipole mass. The parameters a and d are related to the second and fourth moment of the neutron charge distribution respectively [21]

and have the numerical values $a = 0.9$ and $d = 1.75$. As is clear from Fig. 3 (left), our theory agrees well with the $C2/M1$ data at low momentum transfers. In particular, at the real photon point $Q^2 = 0$ we get from Eq.(7) using the experimental neutron charge radius and magnetic moment $C2/M1 = -0.035$, which is in good agreement with determinations of this ratio based on the experimental $E2/M1$ ratio measured in photo-pionproduction and Siegert's theorem relating $E2$ and $C2$ form factors [19].

Moreover, the transition quadrupole moment has been extracted from photo- and electro-pionproduction data as $Q_{p \rightarrow \Delta^+}(\text{exp}) = -0.108(9) \text{ fm}^2$ [24] and $Q_{p \rightarrow \Delta^+}(\text{exp}) = -0.0846(33) \text{ fm}^2$ [25], in good agreement with the prediction $Q_{p \rightarrow \Delta^+}(\text{theory}) = -0.0820(20) \text{ fm}^2$ based on Eq.(5) and the experimental neutron charge radius $r_n^2 = -0.1161(22) \text{ fm}^2$. Concerning the transition quadrupole radius, we obtain from Eq.(6) and experimental values for the radial moments [21] of the neutron charge distribution $r_{C2} = 1.43 \text{ fm}$. The approximate equality $r_{C2} \approx r_\pi$, where r_π is the pion Compton wavelength suggests that r_{C2} measures the spatial extension of the $q\bar{q}$ pair distribution in the nucleon. It would be interesting to determine this radius experimentally.

At higher momentum transfers shown in Fig. 3 (right) the extraction of individual electromagnetic multipoles from the raw cross section data is more difficult as is evident from the difference between the Jefferson Lab [26] and Maid 2007 [22] analyses of the same raw data. The latter analysis, which leads to smaller $|C2/M1|$ (filled circles) than the former (open triangles) is in much better agreement with our theory (dashed-dotted curve). Extrapolating Eq.(7) to $Q^2 \rightarrow \infty$ we find [21]

$$C2/M1(Q^2 \rightarrow \infty) = -\frac{1}{4} \frac{m_N}{m_\Delta} \left(\frac{a}{d} \right). \quad (9)$$

consistent with perturbative QCD, which states that $C2/M1$ asymptotically approaches a small negative constant.

D. Intrinsic quadrupole form factor of the nucleon

For an interpretation of these results it is important to distinguish between the *spectroscopic* and *intrinsic* quadrupole moment of a particle. It is known that a vanishing spectroscopic quadrupole moment does not necessarily imply a spherically symmetric charge distribution. For deformed spin 0 and spin 1/2 nuclei this has led to the general concept of an intrinsic quadrupole moment, which can be defined for different nuclear models. The notion of an intrinsic quadrupole moment allows to interpret measurable quantities such as transition quadrupole moments in terms of the geometric shape of the ground state.

The geometric shape of a spatially extended particle is determined by its *intrinsic* quadrupole moment,

$$Q_0 = \int d^3r \rho(\mathbf{r}) (3z^2 - r^2), \quad (10)$$

which is defined with respect to the body-fixed frame. If the charge density is concentrated along the z -direction (symmetry axis of the particle), the term proportional to $3z^2$ dominates, Q_0 is positive, and the particle is prolate (cigar-shaped). If the charge density is concentrated in the equatorial plane perpendicular to z , the term proportional to r^2 prevails, Q_0 is negative, and the particle is oblate (pancake-shaped).

We calculated the intrinsic quadrupole moment of the proton and Δ^+ in the quark model including two-body exchange currents [9], which effectively describe the quark-antiquark degrees of freedom in the nucleon, and found

$$Q_0^p = -r_n^2, \quad Q_0^{\Delta^+} = r_n^2. \quad (11)$$

Thus, the intrinsic quadrupole moment of the proton is given by the negative of the neutron charge radius and is therefore positive, whereas the intrinsic quadrupole moment of the Δ^+ is negative. This corresponds to a prolate proton and an oblate Δ^+ shape. The model results also suggest that the nonsphericity of the proton charge density is mainly connected with collective quark-antiquark degrees of freedom, the distribution of which has a prolate shape.

The concept of an intrinsic quadrupole moment of the nucleon can be generalized to an intrinsic quadrupole charge distribution and a corresponding form factor [10]. To show this, we first decompose the proton and neutron charge form factors in two terms G_{sym} and G_{def} , coming from the spherically symmetric and the intrinsic quadrupole part of the physical charge density respectively

$$\begin{aligned} G_C^p(Q^2) &= G_{sym}^p(Q^2) - \frac{1}{6} Q^2 G_{def}(Q^2), \\ G_C^n(Q^2) &= G_{sym}^n(Q^2) + \frac{1}{6} Q^2 G_{def}(Q^2). \end{aligned} \quad (12)$$

The factor Q^2 in front of G_{def} arises for dimensional reasons and guarantees that the normalization of the charge form factors is preserved. In coordinate space this corresponds to the usual multipole decomposition of the charge density

$$\rho(\mathbf{r}) = \underbrace{\rho_0(r) Y_0^0(\mathbf{r})}_{\text{monopole}} + \underbrace{\rho_2(r) Y_0^2(\mathbf{r})}_{\text{quadrupole}} + \dots, \quad (13)$$

where the $\rho_0(r)$ part gives rise to $G_{sym}(Q^2)$ and the $\rho_2(r)$ part is connected with $G_{def}(Q^2)$. In terms of fundamental photon-quark processes G_{def} arises mainly from two- and three-quark currents.

For the intrinsic charge quadrupole form factor $G_{def}(Q^2)$ we find

$$\begin{aligned} G_{def}(Q^2) &= -\sqrt{2} G_{C2}^{N \rightarrow \Delta}(Q^2) = \frac{6}{Q^2} G_C^n(Q^2), \\ G_{def}(0) &= -r_n^2 = Q_0^p \end{aligned} \quad (14)$$

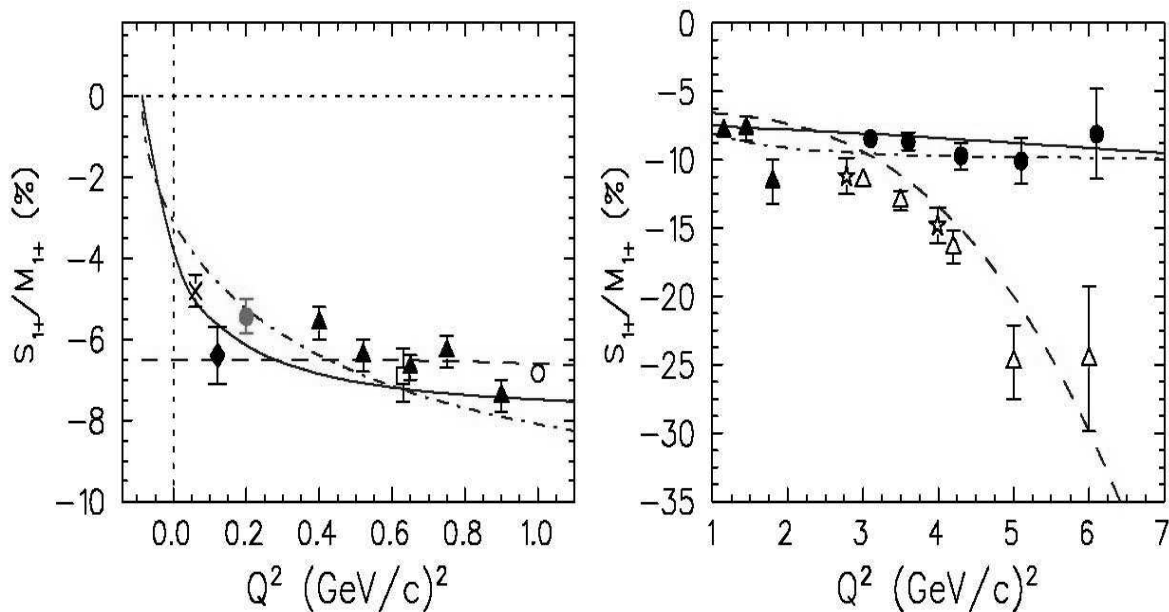


FIG. 3: The $C2/M1(Q^2) \equiv S_{1+}/M_{1+}(Q^2)$ ratio for low (left) and high (right) four-momentum transfers. The full curve is a fit of the experimental $C2/M1$ ratio as determined from the world electro-pionproduction data. The dashed-dotted curve is calculated using the form factor relation of Eq.(7). The open triangles and the dashed curve are from a previous analysis of the same data [26]. Figure taken from Ref. [22].

where we have used Eq.(6). The zero momentum limit follows from l' Hospital's rule and Eq.(11). This shows that $G_{def}(Q^2)$ as defined in Eq.(14) is the proper generalization of the intrinsic quadrupole moment Q_0^p to finite momentum transfers.

To exhibit the effect of the intrinsic quadrupole form factor on the elastic nucleon form factors we insert Eq.(14) into Eq.(12) and obtain

$$G_C^p(Q^2) = G_{sym}^p(Q^2) - G_C^n(Q^2) = \underbrace{G_C^{IS}(Q^2)}_{\text{spherical}} - \underbrace{G_C^n(Q^2)}_{\text{deformed}},$$

$$G_C^n(Q^2) = \frac{1}{6} Q^2 G_{def}(Q^2), \quad (15)$$

where the isoscalar nucleon charge form factor is defined as $G_C^{IS}(Q^2) = G_C^p(Q^2) + G_C^n(Q^2)$ and $G_{sym}^n = 0$. Thus, the relation between the $N \rightarrow \Delta$ and neutron charge form factors of section II B is seen here to have an important implication for the nucleon itself, which can be summarized as: *The neutron charge form factor is an observable manifestation and quantitative measure of the nucleon's intrinsic quadrupole form factor. The latter manifests itself also in the proton charge form factor.*

There are several observable consequences of Eq.(14) and Eq.(15) as discussed in Ref. [10]. At low Q^2 the nucleons's prolate deformation is reflected in a proton charge radius increase by an amount $-r_n^2$, or more directly by a newly introduced size parameter $r_{def}^2 = r_{C2}^2 = (7/10)(r_n^4/r_n^2)$ that can be experimentally determined. At intermediate Q^2 it leads to the conclusion that the dip structure observed in the proton charge form factor [12]

at around $Q^2 \approx 0.2 \text{ GeV}^2$ is due to a corresponding structure in the neutron charge form factor at the same Q^2 . Finally, at high Q^2 it explains the observed decrease of the charge over magnetic form factor ratio [27].

We close this section by stating that our introduction of an intrinsic quadrupole moment and quadrupole form factor of the nucleon should be viewed as an attempt to explore the consequences of the experimental sign and size of the $N \rightarrow \Delta$ quadrupole transition form factor for nucleon ground state structure, which in turn has a bearing on hydrogen hyperfine splitting.

III. HYDROGEN HYPERFINE SPLITTING AND NON-SPHERICAL PROTON SHAPE

A. Fermi energy

It is well known that the ground state energy of atomic hydrogen is split into two levels due to the interaction of the magnetic moments of the electron μ_e and proton μ_p , which can be either aligned ($F = 0$) or antialigned ($F = 1$). The energy difference between these two states is of order 10^{-6} eV which is small compared to the -13.6 eV binding energy of the ground state. For spherically symmetric electronic S states, the magnetic dipole-dipole

interaction Hamiltonian can be expressed as

$$\begin{aligned} H_F &= -\frac{2}{3} \boldsymbol{\mu}_p \cdot \boldsymbol{\mu}_e \delta^{(3)}(\mathbf{r}_p - \mathbf{r}_e) \\ &= \frac{2}{3} (1 + \kappa) \left(\frac{e}{2m_p} \right) \left(\frac{e}{2m_e} \right) \boldsymbol{\sigma}_p \cdot \boldsymbol{\sigma}_e \delta^{(3)}(\mathbf{r}_p - \mathbf{r}_e). \end{aligned} \quad (16)$$

where \mathbf{r}_p and \mathbf{r}_e are the proton and electron position coordinates and $\delta^{(3)}$ is the three-dimensional Dirac δ function. The second equation follows after rewriting the magnetic moments in terms of spin operators as $\boldsymbol{\mu}_p = (1 + \kappa) [e/(2m_p)] \boldsymbol{\sigma}_p$ and $\boldsymbol{\mu}_e = (1 + a) [e/(2m_e)] \boldsymbol{\sigma}_e$. By convention the proton anomalous magnetic moment $1 + \kappa$ is included in the Fermi energy, while the anomalous electron magnetic moment $1 + a$ is included in the QED corrections introduced in sect. III B.

After taking matrix elements of Eq.(16) between hydrogen ground state electron wave functions $\Psi_e(\mathbf{r}_e)$ one obtains for the hyperfine level splitting

$$\begin{aligned} E_F &= \frac{2}{3} (1 + \kappa) \left(\frac{e}{2m_p} \right) \left(\frac{e}{2m_e} \right) \left(\langle \boldsymbol{\sigma}_p \cdot \boldsymbol{\sigma}_e \rangle_{F=1} \right. \\ &\quad \left. - \langle \boldsymbol{\sigma}_p \cdot \boldsymbol{\sigma}_e \rangle_{F=0} \right) |\Psi_e(0)|^2, \end{aligned} \quad (17)$$

where $\delta^{(3)}(\mathbf{r}_p - \mathbf{r}_e)$ has been evaluated for $\mathbf{r}_e = \mathbf{r}_p = \mathbf{0}$ (point nucleon limit). We use the standard normalization N of the hydrogen atom ground state wave function

$$|\Psi_e(0)|^2 = \left(\frac{1}{\sqrt{\pi}} \frac{1}{a_B^{3/2}} \right)^2 = N^2, \quad a_B = \frac{1}{m_r \alpha}, \quad (18)$$

where a_B is the Bohr radius, which is given in terms of the reduced mass $m_r = m_p m_e / (m_p + m_e)$ of the electron-proton system and the fine structure constant $\alpha = e^2 / (4\pi)$. The spin matrix element in Eq.(17) gives $\langle \boldsymbol{\sigma}_p \cdot \boldsymbol{\sigma}_e \rangle_{F=1} = 1$ and $\langle \boldsymbol{\sigma}_p \cdot \boldsymbol{\sigma}_e \rangle_{F=0} = -3$ so that one obtains the Fermi energy formula of Eq.(1) and the numerical value $E_F = 1,418,840.11$ kHz.

B. QED and proton structure corrections to the Fermi energy

It has become customary to express QED and proton structure corrections as parts per million of the Fermi energy, i.e., $1 \text{ ppm} = 10^{-6} E_F = 1.41884$ kHz. The most important corrections to the pointlike dipole-dipole interaction energy in Eq.(1) are due to (i) QED, (ii) nucleon recoil, (iii) finite proton size, and (iv) proton polarization effects [28]. First, there is the anomalous magnetic moment of the electron, which is mainly caused by the QED vertex correction. This and other smaller QED contributions [29] lead to a 1136.1 ppm increase of the theoretical hfs

$$E_{QED}^{HFS} = E_F (1 + \delta_{QED}) = 1,420,452.04 \text{ kHz} \quad (19)$$

to be compared with the experimental value in Eq.(2). One readily notices that there is still a discrepancy between theory and experiment, namely $E_{QED}^{HFS} - E_{exp}^{HFS} = 46.29$ kHz or 32.63 ppm.

Second, adding nucleon structure dependent relativistic recoil corrections $\delta_{rec} = 5.85$ ppm to the theory [30] this discrepancy increases to 38.48 ppm, i.e., a significant deviation by which the theoretical value exceeds the measured one. Third, as a consequence of the proton's finite size, its magnetic moment is distributed over an extended spatial region. This weakens the magnetic interaction with the atomic electron and reduces the hfs. A first estimate of the proton size effect can be obtained from an expansion of the electron wave function for small radial distances $\Psi_e(r) = N \exp(-r/a_B) = N(1 - r/a_B + \dots)$. The spatial extension of the proton magnetic moment distribution is then taken into account by evaluating the electron wave function for $r_e = r_m \neq 0$, where r_m is the proton magnetic radius. This provides a correction term to the Fermi energy of the form [31]

$$E_{proton\ size}^{HFS} = E_F \left(1 - 2 \frac{r_m}{a_B} \right) \quad (20)$$

and the numerical estimate of the proton size effect $-2r_m/a_B \approx -2 \cdot 10^{-5} \text{ \AA} / 0.5 \text{ \AA} = -40$ ppm. When these corrections are added to Eq.(19), one obtains a reduction of the theoretical hfs which is of the right size to achieve agreement between theory and the experimental value in Eq.(2) at the ppm level. The recoil and finite size corrections originate both from second order elastic electron-nucleon scattering depicted by the two-photon exchange diagram in Fig. 4 (left) and are conventionally denoted as δ_{rec} and δ_Z .

Fourth, there are also inelastic contributions (nucleon polarization), which involve intermediate excited proton states, e.g., the $\Delta(1232)$ resonance as shown in Fig. 4 (right). The elastic and inelastic second order electron-proton interaction terms are generically referred to as proton structure contributions. The most important corrections to the Fermi energy are then

$$E_{theory}^{HFS} = E_F (1 + \delta_{QED} + \delta_{rec} + \delta_Z + \delta_{pol}). \quad (21)$$

C. Zemach radius and proton shape

A careful analysis of the proton finite size correction in hydrogen hyperfine splitting was performed by Zemach [5]. Assuming rigid (unpolarizable), spherically symmetric charge and magnetization distributions for the proton, the following expressions were derived

$$\begin{aligned} r_Z &= -\frac{4}{\pi} \int_0^\infty \frac{dQ}{Q^2} \left[G_C^p(Q^2) \frac{G_M^p(Q^2)}{\mu_p} - 1 \right], \\ \delta_Z &= -2 r_Z / a_B \end{aligned} \quad (22)$$

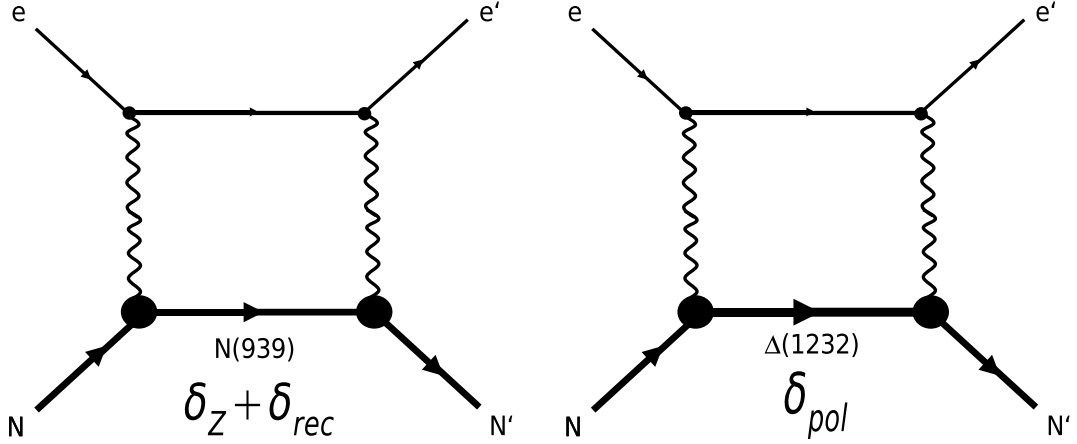


FIG. 4: Two-photon exchange diagrams (crossed photon diagrams are not shown) from which the elastic (Zemach and recoil) and inelastic (polarization) nucleon structure corrections to hydrogen hyperfine splitting are derived. The large black circles represent elastic (left) and inelastic (right) nucleon electromagnetic form factors as measured in electron-nucleon scattering depicted in Fig. 1.

where $G_C^p(Q^2)$ and $G_M^p(Q^2)$ are the elastic charge and magnetic form factors of the proton. In contrast to the estimate in Eq.(20) the Zemach correction δ_Z depends on the details of *both*, charge and magnetic moment distributions. The term -1 in the integrand of Eq.(22) is necessary because the point nucleon limit, $G_C^p(0) = G_M^p(0)/\mu_p = 1$, is already included in the Fermi energy E_F and must be subtracted to avoid double counting. There is also a radiative correction term δ_{rad} due to electronic vacuum polarization [32] which changes $\delta_Z \rightarrow \delta_Z (1 + \delta_{rad})$.

In order to separate the effect of proton's non-spherical charge distribution on the Zemach radius we insert for $G_C^p(Q^2)$ the decomposition of Eq.(15) into Eq.(22) and obtain

$$r_Z = -\frac{4}{\pi} \int_0^\infty \frac{dQ}{Q^2} \left[\underbrace{G_C^{IS}(Q^2) \frac{G_M^p(Q^2)}{\mu_p} - 1}_{\text{spherical}} - \underbrace{G_C^n(Q^2) \frac{G_M^p(Q^2)}{\mu_p}}_{\text{deformed}} \right] = r_Z(sym) + r_Z(def). \quad (23)$$

Thus, the proton Zemach radius is decomposed into two terms coming from the spherically symmetric and non-spherical parts of the proton charge distribution respectively.

For an estimate of the spherically symmetric contribution we assume dipole forms for the isoscalar charge and proton magnetic form factors and obtain the compact

two-parameter formula

$$r_Z(sym) = \frac{3\Lambda_I^4 + 9\Lambda_I^3 \Lambda_M + 11\Lambda_I^2 \Lambda_M^2 + 9\Lambda_I \Lambda_M^3 + 3\Lambda_M^4}{\Lambda_I \Lambda_M (\Lambda_I + \Lambda_M)^3}, \quad (24)$$

which hitherto has not appeared in the literature. Here, Λ_I and Λ_M are the inverse size parameters of the isoscalar charge and proton magnetic form factors. They are related to the corresponding mean square isoscalar charge and proton magnetic radii as $\Lambda_I^2 = 12/r_I^2$ with $r_I^2 = r_C^2(p) + r_C^2(n)$ and $\Lambda_M^2 = 12/r_M^2(p)$. In the limit, $\Lambda_I = \Lambda_M = \Lambda$, Eq.(24) reduces to $r_Z(sym) = 35/(8\Lambda)$, i.e., a standard expression that has been used by several authors [32, 33, 38]. The contribution of the non-spherical part of the proton charge distribution can also be analytically calculated if one uses the two-parameter Galster form of Eq.(8) for $G_C^n(Q^2)$

$$r_Z(def) = -\frac{1}{6} r_n^2 (\Lambda_M m) \frac{16\Lambda_M^3 + 29\Lambda_M^2 m + 20\Lambda_M m^2 + 5m^3}{8(\Lambda_M + m)^4}, \quad (25)$$

where we have used the same dipole mass Λ_M for the proton and neutron magnetic form factors. The quantities r_n^2 and m^2 are related to the Galster parameters a and d as $r_n^2 = 3a\mu_n/(2m_N^2)$ and $m^2 := 4m_N^2/d$. Eq.(24) and Eq.(25) are two main results of this paper.

Inserting experimental values for the dipole parameters Λ_M and Λ_I , as well as for r_n^2 and the Galster parameter $d = 1.75$, one finds the numerical result

$$r_Z = r_Z(sym) + r_Z(def) = 1.0627 \text{ fm} + 0.0464 \text{ fm} = 1.1091 \text{ fm} \quad (26)$$

corresponding to $\delta_Z = -(40.14 + 1.75)$ ppm = -41.89 ppm. The proton deformation contribution is numerically of the same size but of opposite sign as the neutron Zemach radius [34]. The sign change is obvious from the definition in Eq.(23) and the approximate equality in magnitude $r_Z(def) \approx |r_Z(n)|$ follows from the near equality of the normalized proton and neutron magnetic form factors in the relevant moment transfer range. Including the radiative correction gives our final result for the proton Zemach radius $\delta_Z = -41.89$ ppm ($1+0.0151$) = -42.52 ppm. With the Zemach radius contribution included one finds that the discrepancy between theory and experiment reduces to $(38.48 - 42.52)$ ppm = -4.04 ppm.

To obtain a better estimate of the effect of the proton's non-spherical shape on r_Z one would have to determine the proton and neutron charge form factors more accurately in the low momentum transfer region where possible deviations from the smooth dipole and Galster fitting curves may affect $r_Z(def)$ significantly. Electron-proton scattering experiments dedicated to explore this low momentum transfer region with higher precision are being planned [35].

D. Proton quadrupole polarization shift

The proton polarization shift δ_{pol} in hydrogen hfs is caused by two-photon exchange diagrams with nucleon resonances as intermediate states, of which the lowest-lying $\Delta(1232)$ as shown in Fig. 4 (right) is expected to be most important. Here, we focus on those diagrams where one of the photons is a longitudinal charge quadrupole (C2) photon that probes the non-spherical charge distribution in both the ground and excited states.

The polarization shift is usually defined in terms of integrals over the two spin-dependent structure functions $g_1(x, Q^2)$ and $g_2(x, Q^2)$ of the proton, where $x = Q^2/(2m_p\nu)$ is the Bjorken scaling variable and ν is the energy transfer carried by the virtual photon (see Fig. 1). The following formulae for proton polarization in hydrogen hfs have been established [30]

$$\begin{aligned} \delta_{pol} &= \frac{\alpha m_e}{2\pi m_p(1+\kappa)} (\delta_1 + \delta_2), \\ \delta_1 &= \frac{9}{4} \int_0^\infty \frac{dQ^2}{Q^2} \left[F_2^p(Q^2) + \frac{8m_p^2}{Q^2} \int_0^{x_{th}} dx \beta_1(\eta) g_1(x, Q^2) \right], \\ \delta_2 &= -24m_p^2 \int_0^\infty \frac{dQ^2}{Q^4} \left[\int_0^{x_{th}} dx \beta_2(\eta) g_2(x, Q^2) \right], \end{aligned} \quad (27)$$

where $x_{th} = Q^2/(2m_p m_\pi + m_\pi^2 + Q^2)$ is the threshold for one-pion production with m_π being the pion mass, and

the functions $\beta_1(\eta)$ and $\beta_2(\eta)$ are defined as

$$\begin{aligned} \beta_1(\eta) &= \frac{4}{9} \left(-3\eta + 2\eta^2 + 2(2-\eta)\sqrt{\eta(\eta+1)} \right), \\ \beta_2(\eta) &= 1 + 2\eta - 2\sqrt{\eta(\eta+1)}, \end{aligned} \quad (28)$$

with $\eta := \nu^2/Q^2$. Furthermore, $F_2^p(Q^2)$ is the Pauli form factor of the proton, which is defined in terms of the charge monopole and magnetic dipole form factors as $F_2^p(Q^2) = (G_M^p(Q^2) - G_C^p(Q^2))/(1+\tau)$ with $F_2^p(0) = \kappa$ being the anomalous part of the proton magnetic moment. Note that both terms in the integrand of δ_1 diverge for $Q^2 = 0$ but the singularity coming from the second term is cancelled by an analogous singularity of the first term according to the Drell-Hearn, Gerasimov sum rule [36].

The polarization contribution has been calculated by several authors [30, 37]. However, only the contribution of the magnetic dipole (M1) transition to the $\Delta(1232)$ has been studied in some detail. There has been no prior attempt to calculate the contribution of the charge quadrupole (C2) transition to the $\Delta(1232)$. In order to investigate the effect of the latter on the polarization shift, we express the spin structure functions in terms of virtual photon absorption cross sections [39]

$$\begin{aligned} g_1(\nu, Q^2) &= \frac{m_p \nu (1 - Q^2/(2m_p \nu))}{8\pi^2 \alpha (1 + Q^2/\nu^2)} \\ &\quad \left(\sigma_{1/2}(\nu, Q^2) - \sigma_{3/2}(\nu, Q^2) - 2 \frac{Q}{\nu} \sigma'_{LT}(\nu, Q^2) \right), \\ g_2(\nu, Q^2) &= \frac{m_p \nu (1 - Q^2/(2m_p \nu))}{8\pi^2 \alpha (1 + Q^2/\nu^2)} \\ &\quad \left(-\sigma_{1/2}(\nu, Q^2) + \sigma_{3/2}(\nu, Q^2) - 2 \frac{\nu}{Q} \sigma'_{LT}(\nu, Q^2) \right). \end{aligned} \quad (29)$$

Here, $\sigma_{1/2}$ and $\sigma_{3/2}$ are the transverse cross sections with photon-nucleon helicity 1/2 and 3/2, and σ'_{LT} is the longitudinal-transverse interference cross section.

For excitation energies below 1 GeV, which are most important for hydrogen hfs, the cross section is dominated by multipole transitions to specific nucleon resonances and can be written in terms of the helicity amplitudes $A_{1/2}$, $A_{3/2}$, and $S_{1/2}$ as [40]

$$\begin{aligned} \sigma_{1/2} &= 2\pi \frac{m_p}{W} b |A_{1/2}|^2, \\ \sigma_{3/2} &= 2\pi \frac{m_p}{W} b |A_{3/2}|^2, \\ \sigma'_{LT} &= -\sqrt{2}\pi \frac{m_p}{W} \frac{Q}{|\mathbf{q}|} b S_{1/2}^* A_{1/2}, \end{aligned} \quad (30)$$

where W is the total center of mass energy, \mathbf{q} the γN center of mass three-momentum and b the resonance line shape, which at resonance reduces to $b = 2/(\pi\Gamma_{\pi N})$ with $\Gamma_{\pi N}$ being the pion decay width of the resonance. In particular, for $\Delta(1232)$ excitation, the helicity amplitudes can be expressed via the inelastic $N \rightarrow \Delta$ transition form

factors [19] shown in Fig. 1 (right)

$$\begin{aligned}
A_{1/2}(Q^2) &= -\frac{e}{2m_p} \sqrt{\frac{\pi}{K_W}} |\mathbf{q}| \\
&\quad \left(G_{M1}^{N \rightarrow \Delta}(Q^2) - \frac{|\mathbf{q}| m_p}{\sqrt{6}} G_{E2}^{N \rightarrow \Delta}(Q^2) \right), \\
A_{3/2}(Q^2) &= -\frac{e}{2m_p} \sqrt{\frac{3\pi}{K_W}} |\mathbf{q}| \\
&\quad \left(G_{M1}^{N \rightarrow \Delta}(Q^2) + \frac{|\mathbf{q}| m_p}{3\sqrt{6}} G_{E2}^{N \rightarrow \Delta}(Q^2) \right), \\
S_{1/2}(Q^2) &= -e \sqrt{\frac{2\pi}{K_W}} \frac{\mathbf{q}^2}{6} G_{C2}^{N \rightarrow \Delta}(Q^2), \quad (31)
\end{aligned}$$

where $K_W = (m_\Delta^2 - m_N^2)/(2m_\Delta)$ is the energy transfer in the γN center of mass frame at $Q^2 = 0$.

The contribution of the $N \rightarrow \Delta$ charge quadrupole ($C2$) transition form factor to the polarization shift, which comes solely from the σ'_{LT} part in Eq.(29) can now be evaluated. We obtain with $m_N = m_p$

$$\begin{aligned}
\delta_1^{N \rightarrow \Delta}(C2) &= \frac{9}{2} \frac{m_N^3}{m_\Delta^2} \mu_n b \\
&\quad \int_0^\infty \frac{dQ}{Q} \beta_1 \left(\frac{\nu_\Delta^2}{Q^2} \right) G_C^n(Q^2) \frac{G_M^n(Q^2)}{\mu_n}, \\
\delta_2^{N \rightarrow \Delta}(C2) &= -6 \frac{m_N^3}{m_\Delta^2} \mu_n b \\
&\quad \int_0^\infty \frac{dQ}{Q} \beta_2 \left(\frac{\nu_\Delta^2}{Q^2} \right) \frac{\nu_\Delta^2}{Q^2} G_C^n(Q^2) \frac{G_M^n(Q^2)}{\mu_n}, \quad (32)
\end{aligned}$$

where $\nu_\Delta = (m_\Delta^2 - m_N^2 + Q^2)/(2m_N)$ is the resonance energy in the laboratory frame. To derive Eq.(32) we have made use of the form factor relations of sect. IIB and neglected the small $E2 \times C2$ contribution. Numerically, we obtain with values for Λ_M and m as in sect. III C, and $\Gamma_{\pi N} = 0.12$ GeV the following estimates

$$\begin{aligned}
\delta_1^{N \rightarrow \Delta}(C2) &= -0.994 \\
\delta_2^{N \rightarrow \Delta}(C2) &= +0.292 \\
\delta_{pol}^{N \rightarrow \Delta}(C2) &= -0.16 \text{ ppm}. \quad (33)
\end{aligned}$$

The negative sign of the quadrupole polarization shift is indicative of a prolate (cigar-shaped) intrinsic quadrupole deformation of the proton's charge distribution. Interestingly, the charge quadrupole ($C2$) polarization contribution in Eq.(33) is not small compared to the magnetic dipole ($M1$) polarization $\delta_{pol}^{N \rightarrow \Delta}(M1) = -0.12$ ppm derived earlier [37, 38]. Therefore, it will be important to also calculate the polarization shift induced by

transverse electric ($E2$) excitation of the $\Delta(1232)$. Finally, we also give our result for the $M1$ contribution coming from the convergent g_2 integral $\delta_2^{N \rightarrow \Delta}(M1) = -0.69$ ppm compared to $\delta_2 = -0.42$ ppm including additional resonances [37].

IV. SUMMARY

The nonzeroness of the empirical $p \rightarrow \Delta^+(1232)$ quadrupole transition form factor provides evidence that the charge distribution of the proton ground state deviates from spherical symmetry. Employing SU(6) spin-flavor symmetry as a guide we have derived a relation between the $p \rightarrow \Delta^+$ quadrupole transition and neutron charge form factors. It has been shown that this relation agrees with the experimental data from low to high momentum transfers. On this basis, we have proposed that the proton can be assigned an intrinsic charge quadrupole form factor and a positive intrinsic quadrupole moment corresponding to a prolate (cigar-shaped) distribution of the proton charge.

We have then investigated how hydrogen ground state hfs is affected by the proton's non-spherical charge distribution. We have shown that the latter is reflected in a *positive* deformation contribution to the proton Zemach radius, where the increment is given by the modulus of the neutron Zemach radius. A second consequence of the proton's prolate shape is a polarization shift due to the $p \rightarrow \Delta^+(1232)$ charge quadrupole transition that is quantitatively described by the neutron charge form factor. We have presented a numerical estimate for this term and found that it provides a *negative* contribution to the polarization shift in atomic hydrogen hfs that exceeds the one coming from the previously calculated $p \rightarrow \Delta^+(1232)$ magnetic dipole transition.

In view of these results it would be interesting to also explicitly calculate the polarization shift induced by the transverse electric quadrupole form factor $G_{E2}^{N \rightarrow \Delta}$. Because the experimental accuracy of hfs measurements exceeds the theoretical accuracy by several orders of magnitude, hydrogen hfs will remain a high precision probe for proton structure for many years to come. It is quite possible that the interplay between hfs experiment and theory will provide independent evidence for the quadrupole deformation of the proton's charge distribution. Conceivably, hydrogen hfs is also sensitive to higher magnetic multipoles, in particular to an intrinsic magnetic octupole term in the proton's spatial current distribution. We hope to discuss these matters in a future communication.

[1] E. Fermi. Z. Phys. **60**, 320 (1930).

[2] P. J. Mohr, B. N. Taylor, and D. B. Newell. Rev. Mod. Phys. **80**, 633 (2008).

[3] J.E. Nafe, E.B. Nelson, and I.I. Rabi. Phys. Rev. **71**, 914 (1947).

[4] J. Schwinger. Phys. Rev. **73**, 416 (1947); For a histor-

- ical account see: J. S. Rigden. *Hydrogen: the essential element*, Harvard University Press (2002).
- [5] A. C. Zemach. *Phys. Rev.* **104**, 1771 (1956).
- [6] S. D. Drell and J. D. Sullivan. *Phys. Rev.* **154**, 1477 (1967).
- [7] L. Essen, R.W. Donaldson, M.J. Bangham, E.G. Hope. *Nature* **229**, 110 (1971).
- [8] A. M. Bernstein and C.N. Papanicolas. *AIP Conference Proceedings* **904**, 1 (2007); arXiv:0708.0008v1 [hep-ph]; theory review: V. Pascalutsa, M. Vanderhaeghen, S. N. Yang. *Phys. Rep.* **437**, 125 (2007).
- [9] A. J. Buchmann and E. M. Henley. *Phys. Rev. C* **63**, 015202 (2001); A. J. Buchmann and E. M. Henley. *Phys. Rev. D* **65** (2002) 073017; *Eur. Phys. J. A* **35**, 267 (2008).
- [10] A. J. Buchmann. *Can. J. Phys.* **83**, 455 (2005), arXiv:physics/0508007v1 [physics.atom-ph]; *AIP Conference Proceedings* **904**, 110 (2007), arXiv:0712.4270v1 [hep-ph]. Here, the proton and neutron are often generically denoted as nucleon $N(939)$ and the four Δ charge states as $\Delta(1232)$.
- [11] G. G. Simon, F. Borkowski, Ch. Schmitt and V. H. Walther. *Z. Naturf.* **35a**, 1 (1980); S. G. Karshenboim. *Can. J. Phys.* **77**, 241 (1999); I. Sick. *Phys. Lett. B* **576**, 62 (2003); Th. Udem, A. Huber, B. Gross, J. Reichert, M. Prevedelli, M. Weitz, T. W. Hänsch. *Phys. Rev. Lett.* **79**, 2646 (1997).
- [12] J. Friedrich and Th. Walcher. *Eur. Phys. J. A* **17** 607, (2003); hep-ph/0303054; J.J. Kelly, *Phys. Rev. C* **66**, 065203 (2002).
- [13] V. D. Burkert. *Perspectives in the Structure of Hadronic Systems*, ed. M.N. Harakeh et al., Plenum Press, New York, 1994.
- [14] F. Gürsey and L.A. Radicati. *Phys. Rev. Lett.* **13**, 173 (1964); B. Sakita. *Phys. Rev. Lett.* **13**, 643 (1964); M.A.B. Beg, B.W. Lee, and A. Pais. *Phys. Rev. Lett.* **13**, 514 (1964).
- [15] E. Witten. *Nucl. Phys. B* **160**, 57 (1979); R.F. Lebed. *Czech. J. Phys.* **49**, 1273 (1999); nucl-th/9810080.
- [16] G. Morpurgo. *Phys. Rev. D* **40**, 2997 (1989); G. Dillon and G. Morpurgo. *Phys. Lett. B* **448**, 107 (1999); *Europhys. Lett.* **54**, 35 (2001).
- [17] A. Buchmann, Y. Yamauchi, A. Faessler. *Prog. Part. Nucl. Phys.* **24**, 333 (1990).
- [18] D. B. Lichtenberg. *Unitary Symmetry and Elementary Particles*, Academic Press, New York, 1978; F. E. Close. *An introduction to Quarks and Partons*, Academic Press, London, 1979.
- [19] A. J. Buchmann and E. Hernández, A. Faessler. *Phys. Rev. C* **55**, 448 (1997); A. J. Buchmann and E. Hernández, U.Meyer, and A. Faessler. *Phys. Rev. C* **58**, 2478 (1998); U. Meyer, E. Hernández, and A. J. Buchmann. *Phys. Rev. C* **64**, 035203 (2001).
- [20] A.J. Buchmann, J.A. Hester, R.F. Lebed. *Phys. Rev. D* **66**, 056002 (2002); A. J. Buchmann and R. F. Lebed. *Phys. Rev. D* **67**, 016002 (2003); *Phys. Rev. D* **62**, 096005 (2000).
- [21] A. J. Buchmann. *Phys. Rev. Lett.* **93**, 212301 (2004); P. Grabmayr and A.J. Buchmann. *Phys. Rev. Lett.* **86**, 2237 (2001). In the latter paper, we have defined the transition quadrupole radius as $r_{C_2}^2 = -6 d/dQ^2 G_{C_2}(Q^2)$. However, proper normalization requires that the derivative be multiplied by -14 instead of -6, which gives $r_{C_2}^2 = (7/10) (r_n^4/r_n^2)$.
- [22] D. Drechsel, S. S. Kamalov, L. Tiator. *Eur. Phys. J. A* **34**, 69 (2007).
- [23] S. Galster, H. Klein, J. Moritz, K. H. Schmidt, D. Wegener, J. Bleckwenn. *Nucl. Phys. B* **32**, 221 (1971).
- [24] G. Blanpied, M. Blecher, A. Caracappa *et al.*. *Phys. Rev. C* **64**, 025203 (2001).
- [25] L. Tiator, D. Drechsel, S.S. Kamalov and S.N. Yang. *Eur. Phys. J. A* **17**, 357 (2003).
- [26] M. Ungaro *et al.*. *Phys. Rev. Lett.* **97**, 112003 (2006).
- [27] V. Punjabi *et al.*. *Phys. Rev. C* **71**, 055202 (2005); Erratum *Phys. Rev. C* **71**, 069902 (2005); M. K. Jones *et al.*. *Phys. Rev. Lett.* **84**, 1398 (2000); O. Gayou *et al.*. *Phys. Rev. Lett.* **88**, 092301 (2002).
- [28] A. Dupays, A. Beswick, B. Lepetit, C. Rizzo, D. Bakalov. *Phys. Rev. A* **68** (2003) 052503.
- [29] M.I. Eides, H. Grotch, and V.A. Shelyuto. *Phys. Rep.* **342**, 63 (2001).
- [30] C. E. Carlson, Vahagn Nazaryan and Keith Griffioen. arXiv:0805.2603 [physics.atom-ph]; Vahagn Nazaryan, C. E. Carlson, and Keith Griffioen. *Phys. Rev. Lett.* **96**, 163001 (2006).
- [31] S. Fenster and Y. Nambu. *Progr. Theor. Phys. Suppl.*, 250 (1965).
- [32] S. G. Karshenboim. *Phys. Lett. A* **225**, 97 (1997).
- [33] G. T. Bodwin and D. R. Yennie. *Phys. Rev. D* **37**, 498 (1988).
- [34] J. L. Friar and G. L. Payne. *Phys. Rev. C* **72**, 014002 (2005).
- [35] J. Arrington *et al.*. Jefferson Lab PR-07-004 proposal (2007).
- [36] E. De Rafael. *Phys. Lett. B* **37**, 201 (1971).
- [37] R. N. Faustov, A. P. Martynenko and V. A. Saleev. arXiv:hep-ph/9811514v2; R. N. Faustov and A. P. Martynenko. *Eur. Phys. J. C* **24**, 281 (2002); R. N. Faustov, I. V. Gorbacheva, A. P. Martynenko. arXiv:hep-ph/0610332; G. M. Zinov'ev, B. V. Struminskii, R. N. Faustov, and V. L. Chernyak. *Sov. J. Nucl. Phys.* **11**, 715 (1970).
- [38] A. Verganelakis and D. Zwanziger. *Nuovo Cim.* **39**, 613 (1965).
- [39] D. Drechsel, S. Kamalov and L. Tiator. *Phys. Rev. D* **63**, 114010 (2001).
- [40] K. Abe *et al.*. *Phys. Rev. D* **58**, 112003 (1998).